The anatomy of underwater rain noise

Herman Medwin, Jeffrey A. Nystuen,[a] Peter W. Jacobus,[b] Leo H. Ostwald,[b] and David E. Snyder[b]
Physics Department, Naval Postgraduate School, Monterey, California 93943

(Received 3 October 1991; accepted for publication 29 April 1992)

When rain falls onto a large body of water it produces dominating underwater sound over a broad range of audio frequencies. Laboratory studies using more than 1000 single drops, covering the complete size range of actual rain drops at their terminal speeds, have now shown that the complete underwater spectrum of rainfall sound can be dissected into the impact and microbubble sounds produced by four acoustically distinctive ranges of drop diameters D. These are defined as "minuscule" drops ($D \leqslant 0.8$ mm), "small" drops ($0.8 \text{ mm} \leqslant D \leqslant 1.1$ mm), "mid-size" drops ($1.1 \leqslant D \leqslant 2.2$ mm), and "large" drops ($D \geqslant 2.2$ mm). A minuscule raindrop produces only a very weak, almost undetectable, short duration impact noise. A small drop at terminal speed and at local, near-normal incidence, radiates measurable broadband impact sound followed by the very much stronger sound of a "type I" damped microbubble oscillating at frequencies near 15 kHz. A mid-size raindrop radiates only impact sound. Large raindrops, which comprise the major volume of moderate to heavy rainfall, produce an impact sound and a dominating, "type II," "primary" oscillating microbubble of characteristic frequency 2 to 10 kHz depending on the drop diameter. Also, large drops often generate weaker sounds from "secondary" bubbles. The average acoustic energy spectra of large raindrops are distinctive functions of their diameters, the salinity of the surface water, and the temperature difference between the drop and the surface water. When the underwater acoustic intensity spectrum during heavy rain is calculated from the single drop acoustic energy spectra and the drop size distribution, it compares quite well with ocean measurements. The gas injection at the air–water interface is calculated from the probability of bubble formation during a heavy rainfall.

PACS numbers: 43.30.Lz, 43.30.Pc

INTRODUCTION

There have been several attempts to show connections between total rainfall rate and either the overall underwater sound level, or one or two frequencies of the underwater sound spectra measured at sea or in a lake. (e.g., Heindsmann *et al.*, 1955; Bom, 1969; Lemon *et al.*, 1984; Nystuen, 1986; Scrimger *et al.*, 1987, 1989; Tan, 1990; McGlothin, 1991). The physics of the sound producing process is not considered in those papers, although Nystuen did perform the first numerical model analysis of the impact sound.

Franz (1959) conducted the first significant laboratory experiments that lead to predictions of rain noise at sea. By considering individual drops he identified two sources of sound from a water drop falling on a water surface: the short duration impact, and a strongly radiating, damped microbubble, which is sometimes formed several milliseconds later. Such transiently oscillating bubbles (which occur also in breaking waves) have been dubbed "screaming infant microbubbles" (Medwin, 1990) to distinguish them from the nonoscillating, nonradiating "quiescent adult microbubbles," which are commonly found in very great numbers drifting through the near surface ocean.

When a bubble is created, its damped oscillation makes a far stronger contribution to the total underwater sound than the impact source. The bubble, and its size and character, is identified by the time-varying pressure signal radiated. Bubble theory is discussed in Chap. A6 of Clay and Medwin (1977) and Longuet-Higgins (1990).

Franz' research was limited to large drops striking a water surface well below their terminal speeds. To insure applicability of our results to rainfall, we have examined the sound produced by individual water drops for the complete size range of raindrops at their terminal speeds. It is here shown that the sound spectra of rainfall can be dissected into the impact sound or microbubble sound within four acoustically distinctive ranges of drop diameters D. Based on the acoustical output we define "minuscule" drops ($D < 0.8$ mm), "small" drops ($0.8 \text{ mm} \leqslant D \leqslant 1.1$ mm), "mid-size" drops ($1.1 \leqslant D \leqslant 2.2$ mm), and "large" drops ($D > 2.2$ mm).

Only "minuscule" raindrops are close to spherical form at their terminal speeds; "small" drops are close to oblate spheriods (Pruppacher and Pitter, 1971). Meteorologists describe this realm as fog ($D < 0.4$ mm) and drizzle ($0.4 < D < 1.0$ mm). The "mid-size" and "large" drops are deformed oblate spheroids with flat circular bases that become ever larger as the equivalent sphere diameter increases. The "large" drops acquire a concave depression in the base and look kidney-shaped in cross section when $D > 4.0$ mm. (Pruppacher and Pitter, 1971).

The acoustically significant diameter ranges are shown at the bottom of Fig. 1. Throughout this paper the terminol-

[a] Oceanography Department.
[b] Lt., U.S. Navy.

 0001-4966/92/091613-11$00.80

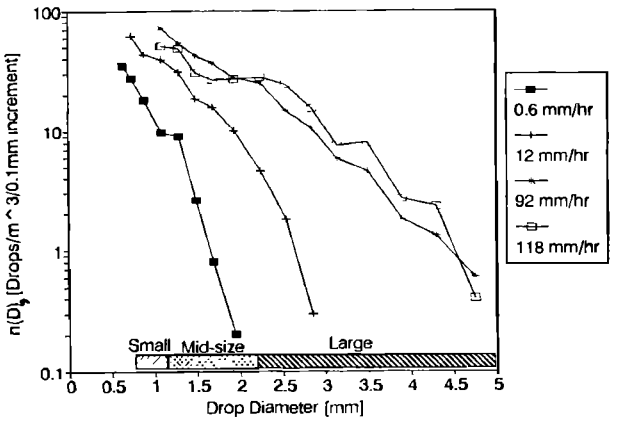

FIG. 1. Raindrop size distributions, $n(D)$ (i.e., number of raindrops per unit volume in 0.1-mm-diam increments) for four rainfalls at Clinton Lake, IL (see Nystuen, 1986). Diameter ranges of small, mid-size, and large drops are indicated at the bottom.

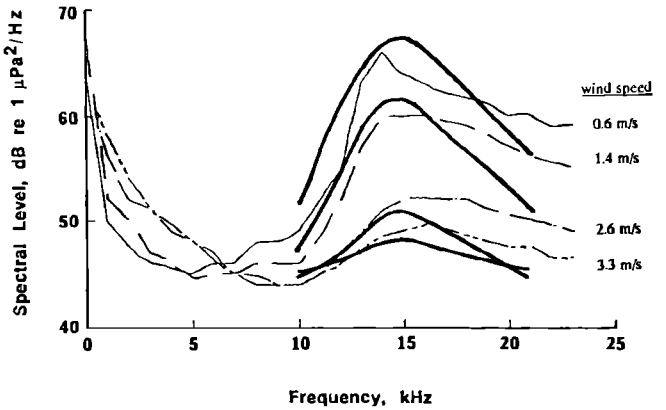

FIG. 2. Field observations (light dashed lines) and predictions (heavy solid lines) based on angles of incidence of small drops at four wind speeds (Nystuen, 1992).

ogy "'small," "mid-size," and "large" drops is used precisely for the diameters that we have defined above; henceforth we omit the quotation marks.

The minuscule raindrop produces only a very weak, almost undetectable, impact noise. It is mentioned here for completeness. A small drop radiates measurable broadband impact sound and the much higher energy sound of a damped microbubble oscillating at peak frequencies around 15 kHz, with peak dipole pressure about 0.4 Pa (at 1 m, on axis).

One hundred percent bubble creation has been verified experimentally for terminal speed, small drops striking a smooth water surface perpendicularly (Pumphrey *et al.*, 1989; Kurgan, 1989; Medwin *et al.*, 1990). It has also been predicted by numerical analysis (Oguz and Prosperetti, 1990) and by fluid dynamic, analytical study (Longuet-Higgins, 1990). The latter authors show that the bubble is formed at the apex of the conical crater, which is produced by the hydrodynamic forces generated by the vertical impact of a small drop onto a smooth, horizontal surface. We call this a "type I" process. The oscillating bubble caused by this process has sometimes been proposed as the sole source of rain noise at sea.

When wind is present, it imparts a significant horizontal velocity to the small raindrops. This, or the prior existence of a rough surface, tends to make drops impact the surface locally at oblique angles. Laboratory studies (Medwin *et al.*, 1990) have demonstrated that bubble creation for small raindrops decrease from 100% at normal incidence to 10% at 20° with the normal. Since a near-surface wind speed of only 1.3 m/s is capable of carrying small raindrops to a 20° angle of entry, even light winds will reduce the probability of bubble formation. A small rms slope of the water surface can do the same. Nystuen (1992) studied the surface slope and wind effects and was able to obtain very good predictions of the underwater sound from a knowledge of wind speed alone during realistic light rain conditions (see Fig. 2).

Laville *et al.* (1991) attribute rainfall noise solely to bubbles and impacts from small drops. They claim "the direct observation of heavy rain...dismisses bubbles associated with large drops as a significant contributor to the general level." In fact, the heaviest rain reported by Laville *et al.* is 6 mm/h, which is " moderate" rain according to the *Glossary of Meteorology* (1989). Figure 1 suggests that there are probably no large drops (as we define them) in the Laville experiment.

Moderate or heavy rainfalls contain mostly drops of diameter greater than 1.1 mm. Before Snyder (1990) no laboratory or theoretical research had been attempted for these raindrops at their terminal speeds. We show that a mid-size raindrop, ($1.1 < D < 2.2$ mm) produces only a short duration, broadband, impact sound when it hits the water.

Photos of large drop splashes were first shown by Worthington (1908).

A large raindrop that is normally incident at terminal speed on smooth water produces both impact sound and strongly radiating bubbles. We call this a "'type II" process. It includes a strong "primary" type II bubble and often weaker, "secondary" bubbles. We will show that these type II bubbles determine the rainfall sound over a broad range of frequencies below 10 kHz during heavy rainfall.

I. RAINFALL RATES AND DROP SIZE DISTRIBUTIONS

Since we will be using the sound produced by single drops to interpret the total underwater sound for a given rainfall condition, we first consider the relations between rainfall rate (mm/h), drop size distribution, and drop rate density (number of drops per m^2/s). The total rainfall rate TRR (depth of rainfall per unit time) can be expressed in terms of the number of drops per unit volume $n(D)dD$ before the rain strikes the surface, the water volume per drop $\pi D^3/6$, and the terminal speed V_T,

$$\mathrm{TRR} = \int_D \frac{\pi}{6} D^3 n(D) V_T(D) dD. \tag{1}$$

Using the mixed units favored by meteorologists to fit the resolution of their measuring instruments, this is

$$\mathrm{TRR(mm/h)} = 6\times 10^{-4} \int_0^{5\ \mathrm{mm}} \pi D^3 n(D) V_T(D) dD, \tag{2}$$

where D has units mm, $n(D)$ has units (m^{-3}) ($0.1\ \mathrm{mm}^{-1}$),

dD is the drop diameter increment in units (0.1 mm), and $V_T(D)$ is the terminal speed (m/s). The integration is extended to 5 mm because that is commonly the largest diameter in rainfall. It is useful to note that the *Glossary of Meteorology* (1959) defines the terminology "light" rain for TRR < 2.5 mm/h, "moderate" for 2.5 mm/h < TRR < 7.6 mm/h, and "heavy" for TRR > 7.6 mm/h.

Theoretical curves for terminal speed were given by Pruppacher and Klett (1978). Snyder (1990) has verified that for these drops of equivalent diameter 2.2 to 4.6 mm the terminal speed V_T is described by

$$V_T \approx 4.6\sqrt{D}. \tag{3}$$

Using this relation, the contributing rainfall rate for large drops RR_L is given by

$$RR_L(\text{mm/h}) = 2.8\times 10^{-3}\pi \int_{2.2\text{ mm}}^{4.6\text{ mm}} D^{7/2} n(D)\,dD. \tag{4}$$

It is useful, also, to calculate the drop rate density, that is the number of drops per square meter, per second, DRD. This can be done for the different types of drops by integration. For example, for small drops it is given by

$$DRD_s = \int_{0.8\text{ mm}}^{1.1\text{ mm}} V_T(D) n(D)\,dD. \tag{5}$$

Some drop size distributions are shown in Fig. 1. They were obtained during a convective storm over Lake Clinton, IL (Nystuen, 1986). The drop diameter resolution ranged from $\pm$ 0.1 mm for diameters 0.3–0.8 mm, to $\pm$ 0.5 mm for diameters 4.5–5.6 mm. In Table I, the drop rate densities and contributing rainfall rates (mm/h) are given for small drops, mid-size, and large drops during light, heavy, and very heavy rain, as calculated from three of the curves in Fig. 1. Table I shows that mid-size and large raindrops constitute the major portion of the total water volume in rain, when they are present. This emphasizes the need to study the sound produced by these drop sizes if accurate rainfall rate predictions are to be made using underwater sound.

The drop size distributions in rainfall have been generalized in the empirical Marshall–Palmer (1948) relation that predicts that the distribution will have an exponential dependence on drop diameter, e.g., the 0.6- and 92-mm/h curves of Fig. 1. In fact, deviations from exponential behavior are common, e.g., the 12- and 118-mm/h curves of Fig. 1. Furthermore, Beard *et al.* (1986) show that there are many more of the large diameter drops than would be predicted by the Marshall–Palmer distribution when TRR > 10 mm/h in rain from warm, shallow, convective clouds. These variations in DSD again emphasize the need to study the dependence of the sound spectrum on the drop size if accurate rainfall rate predictions are to be made from underwater sound.

TABLE I. Contributing rainfall rates (mm/h) due to small, RR_s, mid-size, RR_m, and large, RR_l, drops for examples of light (0.6 mm/h), moderately heavy (12 mm/h), and very heavy rainfall (92 mm/h) from Fig. 1. Drop rate densities (number of drops per meter^2 per second) for small, DRD_s, mid-size, DRD_m, and large drops DRD_l are in parentheses.

	Light rain	Heavy rain	Very heavy rain
$RR_s(DRD_s)$ small drops	0.36(88.6)	1.06(621)	2.13(1278)
$RR_m(DRD_m)$ mid-size drops	0.22(16.4)	8.62(1203)	23.08(2732)
$RR_l(DRD_l)$ large drops	none	3.61(139)	67.5 (1238)
TRR(DRD)	0.6 (105)	12 (1963)	92 (5248)

II. EXPERIMENTAL DETAILS

A. Physical setup

The Naval Postgraduate School has a unique facility for raindrop sound research: a 3-×3-×26-m vertical utilities shaft with a 1.5-m deep×1.5-m-diam anechoic tank at its bottom. The 26-m fall allows large drops (< 4.8 mm diameter) to reach terminal speeds at impact (Snyder, 1990). This "drop tower" was used for all the large and mid-size drop experiments.

The anechoic tank is a cylindrical, redwood barrel with dimensions 1.5-m height and 1.5-m diameter modified by an inner "lining" constructed of 10 and 5 cm square and triangular cross-section redwood wedges. With the lining in place, there was a minimum of 7-dB reduction in reverberation noise at 3 kHz and 22-dB reduction at 20 kHz. Tap water was used for the fresh water experiments. To provide synthetic ocean water containing 35 ppt salinity we added 108 lb of *sea salt*, manufactured by Lake Products Co. We have also used filtered seawater. The salinity content was measured by an AGE model 2100 salinometer with an accuracy of 0.05 ppt.

An Eppendorf digital micropipette (model 4710, 0.5–10.0 μl) with a published volume accuracy of $\pm$ 1% was used for the 2.2- to 2.7-mm drop diameter range. For drops in the range 2.7- to 3.6-mm diameter, an Eppendorf digital micropipette (model 4710, 10–100 μl) with a volume accuracy also of $\pm$ 1% was employed. For drops with a diameter greater than 3.6 mm, individually calibrated glass eye droppers were used. The accuracy of the eye droppers was measured to be $\pm$ 5% by volume. The accuracy was also verified by a precision balance to be $\pm$ 5% by mass for each individual drop. In the later work, a standard medical, intravenous, drop bag was used to feed a calibrated glass eye dropper that produced a stream of separated drops with an adjustable drop rate. Again, the mass accuracy was $\pm$ 5% for each individual drop. We note that none of these drops are spherical at their terminal speeds; the *equivalent* diameters that we report are calculated from the spherical volumes and have an equivalent diameter accuracy which is 1/3rd of the mass accuracy, i.e., better than 2%.

B. Data acquisition and signal processing

The hydrophone consisted of two 3.2-mm-diam hollow coaxial cylindrical barium titanate elements. It was calibrated by both the spherical reciprocity and comparison methods. Its response was flat $\pm$ 2 dB from 1 to 300 kHz. It was positioned at 15-cm depth for the early work and 6-cm depth (with a correction for near field) for the later work. The

increased signal-to-noise ratio at close range provided a much cleaner signal, particularly for the impact sound.

The signal for the hydrophone was amplified by a PAR 113 low noise pre-amplifier with a gain of 2000, then passed through two Krohn–Hite bandpass filters with a pass frequency band of 2- to 30-kHz with a total roll-off of 48 dB per octave. When there was less noise the signal was fed to a single Krohn–Hite 3202R band pass filter, passing frequencies between 1 to 300 kHz for impact signal acquisition and 1 to 30 kHz for bubble signal acquisition. The effect of a filter on the radiation of the relatively minor impulse sound has been considered by Nystuen *et al.* (1992).

A digital data acquisition card (Computerscope, RC Electronics) was mounted in an IBM PC/XT for acoustical data acquisition. It is capable of sampling frequencies up to 1 MHz at an amplitude resolution of 12 bits. The temporal resolution given by the 1-MHz sampling frequency was used for the impact signals. The 250-kHz sampling frequency with a longer record length was used for all of the bubble data samples.

Motion pictures of 4.6-mm drops impacting the water surface at their terminal speed of 9 m/s were taken with a 400 frame per second Milliken camera. The individual frames were studied with a "stop-frame" projector. Slow motion was achieved by re-recording on VHS video recorder at a factor of 1000 slowdown.

Both the impact and bubble signals were corrected to an equivalent far-field pressure at 1 m on the vertical axis below the drop impact point by taking into account the spherical spreading as well as the $\cos\theta$ dependence of dipole radiation. The bubble radiation dipole pattern has been confirmed for smaller, terminal speed drops at normal incidence (Kurgan, 1989). The dipole character of the impact has been confirmed by Ostwald (1992).

The near-field effect correction factor has been derived by Medwin and Beaky (1989). The magnitude correction is

$$p_{ff} = p_{nf}(1 + 1/k^2r^2)^{-1}, \tag{6}$$

where p_{ff} is the far-field pressure and p_{nf} is the near-field pressure, k is the wave number in m^{-1}, and R is the range from hydrophone to impact position in m. For the frequencies of interest, the near-field correction was not always necessary but, for convenience, it was used for the hydrophone at any depth.

The *bubble* temporal voltage signal was sampled at 250 kHz for 8.2 or 16.4 ms depending on the time necessary to obtain 99% of the total energy of the decaying sinusoid. After windowing, the signal was converted to its frequency spectral components by a 2048-point fast Fourier transform. Box-car windowing was used because it yields essentially the same spectrum as an analytical Fourier transform of an infinite duration damped sinusoid (Ostwald, 1992). By using the sensitivity of the hydrophone (V/μPa) we obtain a quantity with units $\mu Pa^2s/Hz$ that we call the "sound energy spectral density" because it is proportional to $J\,m^{-2}\,Hz^{-1}$. (*Note*: this is *not* the intensity spectral density that is commonly calculated for continuous, random sounds at sea, see Ostwald, 1992.)

On the other hand, the impact *impulse* record length that had a duration of $< 100\,\mu s$ was sampled at 1 MHz for $256\,\mu s$, long enough to capture 99% of the impact sound for all drop diameters. The total energy of the impact or the bubble radiation is obtained by integration over the hemisphere, assuming a dipole radiation pattern.

Individual bubbles and impacts were processed sequentially and yielded an output of energy spectral density versus frequency at 1 m on axis. Each drop event was evaluated for frequency of the peak energy density and the presence or absence of signals from the secondary bubbles.

As large drops fall they "wobble," so that their axes are generally not parallel to the direction of travel. The irregular entry of wobbling, nonspherical drops results in sound radiation that varies from one drop to the next. For each drop of the same category (e.g., all 4.6-mm drops at a particular temperature and salinity) we average the spectra in both frequency and ensemble. The frequency average consists of a 1-kHz-wide moving filter applied to smooth the individual spectra (which contain impact energy and both primary and secondary bubble radiation). The ensemble average is applied to all drops of the same category. The distributions and standard deviations of the spectral levels at the dominant bubble frequency and of the total energy per raindrop have been presented by Jacobus (1991) and Ostwald (1992).

C. Calculation of spectrum levels due to rainfall

The research described here yields the source energy spectral densities 1 m below the water surface, caused by terminal speed single drops. In order to calculate the underwater sound intensity spectral densities during a rainstorm it is necessary to specify the drop size distribution $n(D)$ either by having simultaneously measured the quantity with a distrometer, as in Fig. 1, or (by default) by knowing the total rainfall rate in mm/h and assuming a Marshall–Palmer distribution. One assumes a uniform distribution of drops over the water surface. For the ith diameter of a known drop size distribution $n(D_i)$ reaching the surface at its terminal speed $V_T(D_i)$ one then use the average energy spectral density per raindrop SD_e at frequency f_j, to obtain the calculated rainfall spectral density at that frequency $RS(f_j)$ 1 m on axis. Because of the dipole radiation pattern it is necessary to use the geometrical factor $R^{-2}\cos^2\theta$ for a drop at distance R from the hydrophone and range r from drop to epicenter. The angle to the source is given by $\sin\theta = r/R$. Analytically, the rainfall spectrum is

$$RS(f_j) = \sum_i \int_0^{r_o} V_T(D_i)n(D_i) \times SD_e(f_j,D_i)\frac{\cos^2\theta}{R^2}2\pi r\,dr, \tag{7}$$

where i is the drop diameter bin, j is the sound frequency bin, and r_o is the outermost surface radius sensed by the hydrophone. Changing to θ integration by using $\sin\theta = r/R$ we have the spectrum received by a point hydrophone,

$$\mathrm{RS}(f_j) = \sum_i \int_0^{\pi/2} V_T(D_i) n(D_i) \mathrm{SD}_e(f_j, D_i) \times 2\pi \cos\theta \sin\theta \, d\theta. \quad (8)$$

Performing the integration,

$$\mathrm{RS}(f_j) = \sum_i \pi V_T(D_i) n(D_i) \mathrm{SD}_e(f_j, D_i). \quad (9)$$

To convert to rainfall spectrum level,

$$\mathrm{RSL}(f_j) = 10 \log_{10} \mathrm{RS}(f_j). \quad (10)$$

Therefore, for uniformity distributed dipole sources on the surface the underwater rainfall sound spectrum is independent of the depth of the free field hydrophone if there is no bottom interaction and if attenuation in the volume is neglected. However, for comparison with field measurements there must be a correction for the reflection or scattering caused by the usual bottom mounting. Also there is undoubtedly a bubble distribution under the water surface that would need to be measured in order to calculate the sound level at depths below the surface. This latter correction has been considered by others, e.g., Lemon *et al.* (1984).

III. SMALL RAINDROPS ($0.8 \leqslant D \leqslant 1.1$ mm): IMPULSE AND BUBBLE

Because of the prominent 15-kHz component that has been observed, particularly during light rain, almost all of the drop research in the past has been conducted on small drops and light rainfall (see references in Introduction). The typical signal for a small drop consists of an impulse that lasts for less than 10 μs followed, about 20 ms later, by an exponentially damped sinusoid due to a damped bubble. We call the bubbles "type I" to distinguish them from those generated by large drops at terminal speeds. Here, we summarize the findings for small drops (Medwin *et al.*, 1990).

A. At normal incidence

(a) A small drop produces a bubble 100% of the time.

(b) The impact peak pressure is 0.14 Pa; the bubble peak pressure ranges from 0.4 to 0.55 Pa.

(c) The resonance frequency of the bubbles ranges from 12 to 21 kHz, with average value 15.5 kHz and standard deviation 1.7 kHz.

(d) The energy of the impact sound is 0.012 ± 0.003 pJ; the energy of the bubble sound is 1.9 ± 0.4 pJ.

(e) The radiation pattern is dipole.

B. At oblique incidence

(a) The percentage of drops that create bubbles decreases from 100% at normal incidence at 10% at 20° incidence.

(b) The resonance frequency of the bubbles (when created) increases from about 14 to 17 kHz as the incidence changes from normal to 20°.

(c) The impact energy increases from 0.01 to 0.017 pJ as the incidence changes from normal to 40°.

(d) The radiation pattern is approximately dipole.

Small drops are the major components of light rains (e.g., the case where the total rainfall rate is 0.6 mm/h in Table I). Consequently, the type I bubbles from small raindrops are the primary sound sources during light rainfall. However, the strong dependence of the bubble creation percentage on the angle of incidence means that the acoustic energy output of the small drops will be sensitive to the presence of winds and the slope of the water surface on which the drop falls. This has been seen in the sound spectra of Nystuen and Farmer (1987) and in Laville (1991) and has been analyzed by Nystuen (1992) from single drop data. See Fig. 2.

IV. MID-SIZE RAINDROPS ($1.1 \text{ mm} \leqslant D \leqslant 2.2$ mm): IMPULSE AND NO BUBBLE

When drops of equivalent diameter 1.1 to 2.2 mm strike the water surface we find that they do not create bubbles. This is because their speed is too great to create the proper conical crater as described by Oguz and Prosperetti (1990) and Longuet-Higgins (1990), and we speculate that their kinetic energy is too small to create the jet phenomenon and bubble creation described for large drops in the next section. The fact that they radiate only impact energy has been verified by observing 50 mid-size drops, 25 of diameter 2.2 mm, and 25 of diameter 2.0 mm. No bubbles were detected.

The impact component of a raindrop has been described by Franz (1959); Nystuen (1986); Oguz and Prosperetti (1991); Guo and Ffowcs-Williams (1991); Pumphrey and Elmore (1990); Pumphrey and Crum (1990); Snyder (1990); and Nystuen *et al.* (1992). Snyder showed that in the case of a large drop, sampled at 1 MHz, there are prominent aspects of the impulse signal that can be attributed to internal reflections within the raindrop as it strikes the surface. This is shown in Fig. 3.

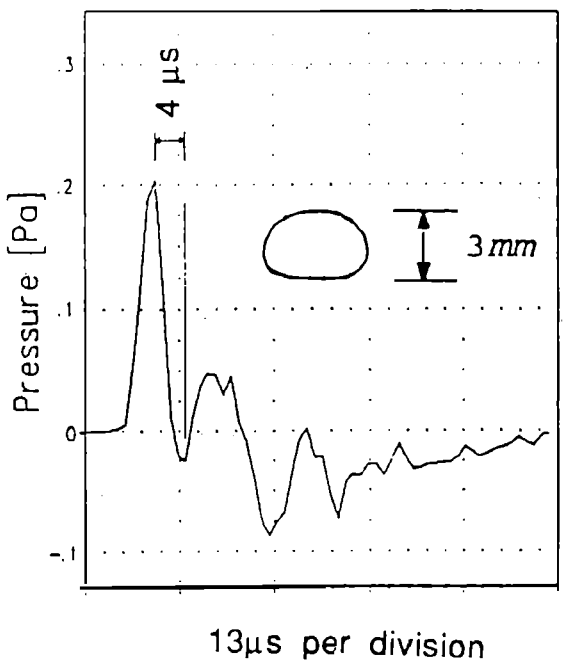

FIG. 3. Impact signal from a 4.6-mm drop. The first pressure minimum, 4 μs after the peak, is attributed to the drop interior pulse that is phase-shifted at the top of the drop. See Snyder (1990) and Nystuen *et al.* (1992).

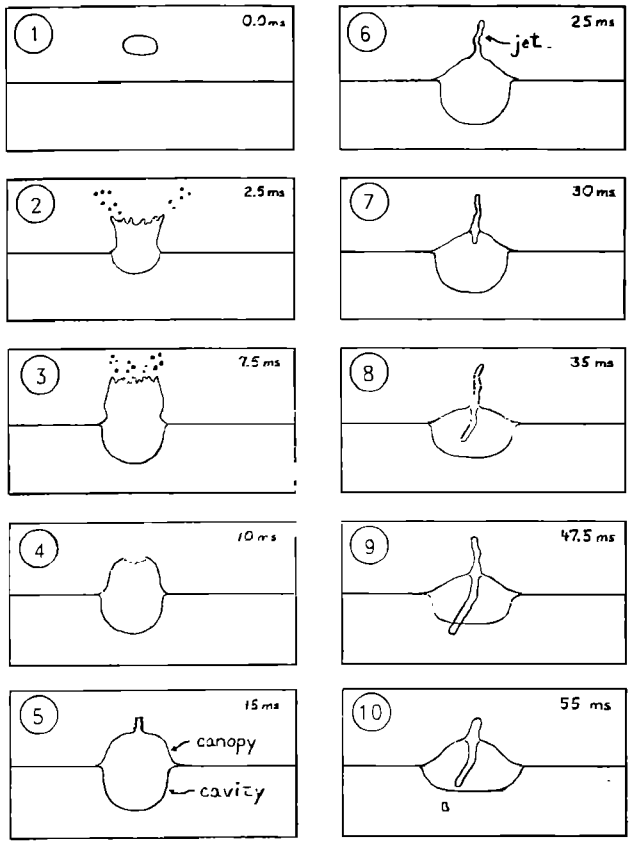

FIG. 4. Stages of hydrodynamics of a 4.7-mm terminal-speed, large drop striking a water surface at normal incidence.

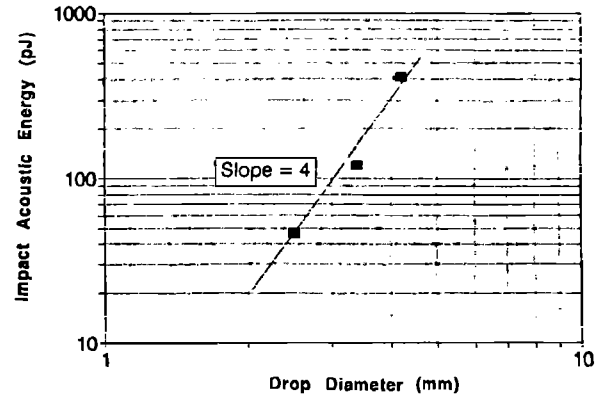

FIG. 5. Average acoustic energy of impact for terminal-speed, large drops in 35 ppt salt water. Several hundred drops used.

V. LARGE RAINDROPS ($D \geqslant 2.2$ mm): IMPULSE AND BUBBLES

A. Sound production

We have recorded the sound produced by almost 2000 large raindrops and have viewed high-speed motion pictures (400 frames/s) of about 40 drops. The visual observations allow us to describe the physical origins of the acoustical signals at the measured delay times.

Figure 4, from Snyder (1990), shows sketches of the significant stages of the hydrodynamics of a large drop splash on a smooth water surface. The events are very different from the hydrodynamics of a small drop splash. The time between consecutive frames was 2.5 ms; the frames shown were selected for their significance in the sound-generating process.

The first frame shows the drop slightly prior to impact. The 4.7-mm-diam drop is not spherical but is concave on the bottom as described by Pruppacher and Pitter (1971). The impact, which is the first acoustical evidence of the drop, has been missed by the 2.5-ms spacing of the frames.

For large drops the terminal speed is proportional to $D^{1/2}$ and therefore the kinetic energy at impact is proportional to D^4. Figure 5 shows that the acoustic energy is also proportional to D^4. The fraction of the large drop kinetic energy converted to impact acoustic energy is approximately 2×10^{-7}.

In some very few cases (less than 5% of large drops) an oscillation of a bubble is detected *immediately* following the impact (Fig. 6). From the change of frequency we assume that this is due to air caught in the concave bottom of the drop and squeezed out as the oscillation damps.

The next frame of Fig. 4 shows the formation of the crown and the beginning of a *hemispherical* crater in the water about 2 ms after impact. A spray of droplets is ejected by the upward moving water mass. A canopy is formed.

After the canopy closes, a jet that is fed by water moving up the canopy, rises to a height of 2.9 ± 0.3 cm at a time 25–30 ms after impact. From Fig. 4, its average speed is estimated to be about 100 cm/s. Then a downward jet appears at the peak of the canopy. In stages 7 and 8 of Fig. 4 it plunges downward, at a speed estimated at 200 cm/s. The next frame shows the jet piercing the bottom of the flat-bottomed crater. It is after this time that a dominant bubble signal is often detected; we call this a type II primary microbubble (Fig. 7). In our observations the presence of the cant (angle) in the jet has always coincided with the release of a microbubble (frame 10). This appears to be due to buoyant forces that act

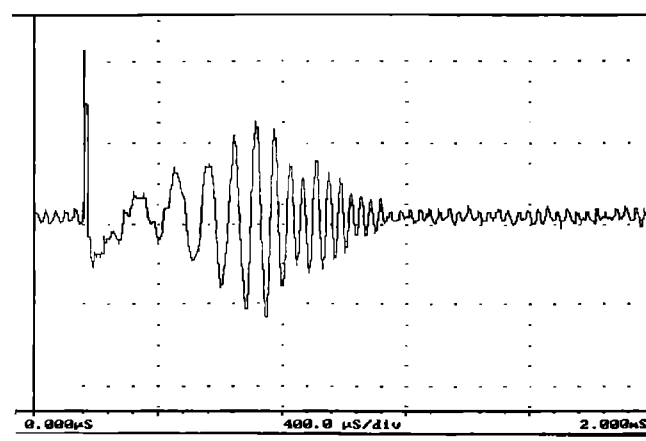

FIG. 6. Signal from an oscillating bubble immediately after impact of a large drop in fresh water. The bubble frequency increases from 10 to 30 kHz.

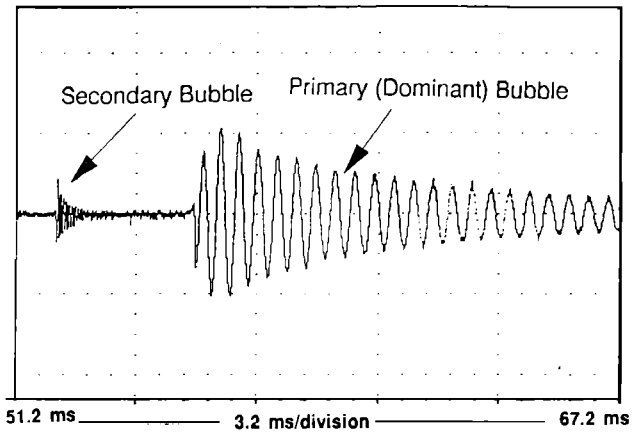

FIG. 7. Acoustical signal of a primary type II bubble and an early secondary bubble caused by a large drop splash in fresh water.

on the air trapped at the end of the jet. Delay times from the impact to the onset of the dominant bubble sound range from 35 to 65 ms (Fig. 8), being larger for the larger drops.

For some of the drops there is also a weaker "secondary" bubble radiation due to a smaller bubble (Fig. 7). The bubble identification is made by measuring the damping constant and frequency of the oscillation (Clay and Medwin, 1977). From the observed time delays (relative to the impact) it is possible that the secondary bubble is caused by a splash droplet hitting the water at the proper speed and angle. It is more likely that a secondary bubble is trapped in one of the interstices of the jet. Similar actions have been described by Scott (1975) for larger jets. We have observed that the surface of the jet appears to be rough and that its Reynolds number $\mathscr{R}$ is greater than 1000 when calculated from the average speed and jet dimensions in the photographic evidence. It is known (Schlichting, 1960) that a constant speed water jet of $\mathscr{R} > 30$ becomes turbulent and picks up gas from the surrounding air.

Because the cant of the microjet appears to be a requirement for type II bubble formation, we speculate that drops incident at oblique angles, due to wind or surface roughness,

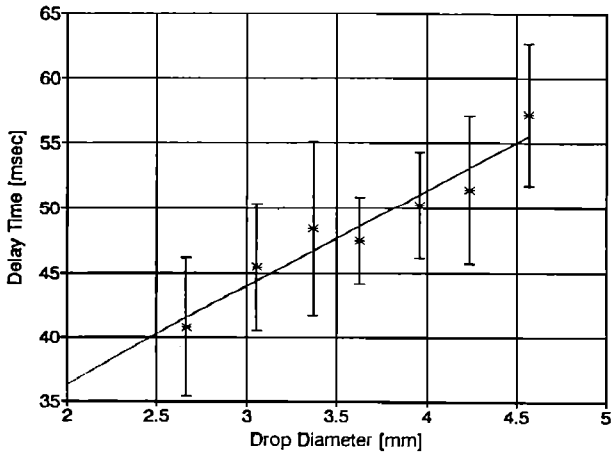

FIG. 8. Delay times between large drop impact and onset of a primary type II bubble in fresh water (300 drops used).

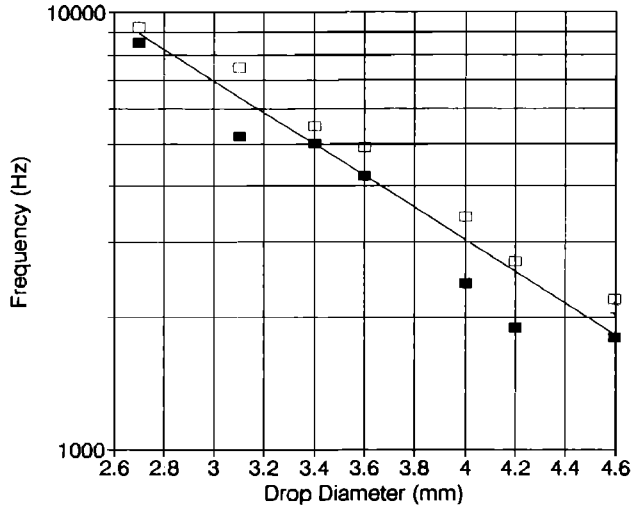

FIG. 9. Frequency dependence of the peak of the spectral density for large drops in fresh water. Closed squares are from Snyder (1990), open squares are from Jacobus (1991) (300 drops used).

could have a *higher* percentage of primary bubble production than normally incident drops. This is in contrast to the situation for type I bubble creation. We know of no research on the sound radiation from terminal-speed, large drops at oblique incidence to the water surface or incident on a locally rough water surface.

B. Frequencies of type II primary bubbles

An important discovery is that when a primary bubble is produced it has a peak frequency that is inversely proportional to the volume of the large raindrop that caused it. The data are shown in Fig. 9. An approximate empirical relation for range 2–10 kHz is

$$f = (160/D^3) + 0.6, \tag{11}$$

where f is the frequency of the primary bubble in kHz and D is the drop diameter in mm. Furthermore, since the terminal speeds of large drops are approximately constant, $\pm$ 10%, the primary bubble frequency is approximately inversely proportional to the kinetic energy of the impacting large drop.

C. Average energy spectral densities of drops

Not all large drops produce bubbles, which are the principal components of the radiating acoustic energy when they are present. The percentage production of primary bubbles for normal incidence of large drops in fresh water is shown in Fig. 10. The percentage in saltwater is almost the same. A still smaller percentage of drops produce secondary bubbles. In Fig. 10, the 0% value for drops of diameter 2.2 mm is the criterion that we have selected to define the smallest diameter of what we call a "large" (bubble-producing) drop.

To calculate the average acoustic energy spectral density for a given drop diameter it is necessary to add the contributions at each frequency of the spectrum, whether or not bubbles are created. Our laboratory research for fresh water used 50 drops of each of 7 diameters. For salt water, over 500 drops were used to yield the energy spectral densities shown in Fig. 11.

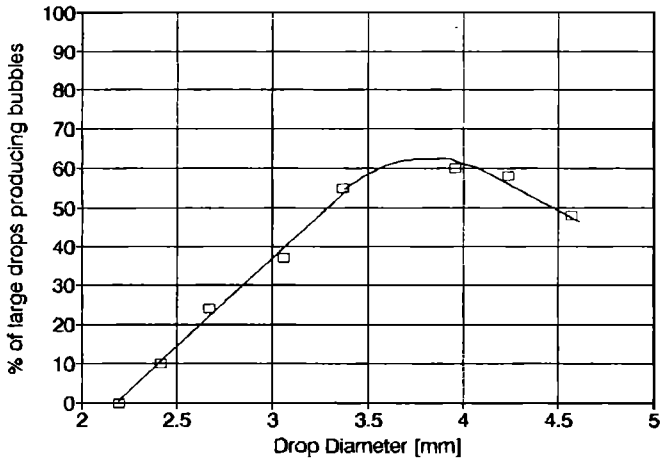

FIG. 10. Percentage of large drops that produce primary type II bubbles in fresh water (over 700 drops used).

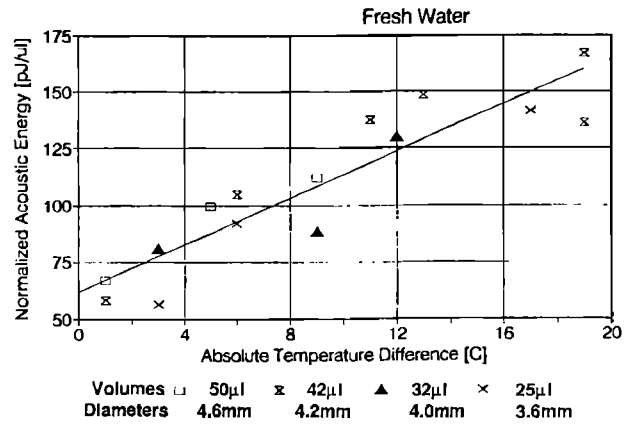

FIG. 12. Additional energy per unit drop volume due to drop-surface absolute difference of temperature in fresh water. The largest temperature difference (19 °C) was achieved by tank water temperature 21 °C and drop temperature 40 °C or 2 °C (over 700 drops used).

The breadth of the spectral peak of the average radiation from a drop can be defined as $Q' = f/\Delta f$, where Δf is the — 3-dB frequency range. Values of Q' from about 1 to 3 are obtained from Fig. 11. This contrasts with the much higher Q that ranges from about 15 to 30 for single bubbles at these peak frequencies (Clay and Medwin, 1977). The lower values of Q' are of course due to the range of bubble radii that occur for large drops.

D. Effect of temperature

The study of sound radiation dependence on temperature produced unexpected results (Jacobus, 1991). We had expected that there would be a small monotonic temperature effect due to the dependence of bubble radiation on surface tension and viscosity. What we found was that the acoustic energy per unit drop volume showed a significant dependence on the *absolute difference* of temperature of drop and surface waters. The results are in Fig. 12.

Noting that the increased energy is proportional to the drop volume, we speculate that there is an increase in the Helmholtz free energy of the raindrop and surface-entrained waters during the turbulent mixing process, and that a fraction of that Helmholtz free energy is released in the form of additional acoustic energy. Although such a process would be quite inefficient, it seems possible when we consider that only about 10^{-6} of the kinetic energy of the drop goes into total acoustic radiation, so that a very small change in the efficiency of the conversion would be detectable acoustically. Measurements by Scofield (1992) show that the increased energy at higher temperature differences is due to increased amplitudes of oscillation of the damped sinusoids.

Figure 12 shows that this temperature dependence may be a significant effect for rainfall at sea. Furthermore, one may speculate that it might even be possible to predict the level of the clouds from which the rain has fallen from a knowledge of the surface water temperature. Preliminary calculations (Kamada, 1992) show that such a remarkable inference about clouds, based on near surface underwater sound levels, is feasible if certain assumptions are made about the air mass through which the drops have fallen.

McGlothin (1991) has observed that for *the same heavy rainfall rate* (near 100 mm/h) the spectral levels were about 4 dB higher during increasing rates at the beginning of convective storms than during the decreasing rates at the end of the storms. The obvious guess is that there was a change in drop size distribution. Another possibility is that there was an accumulation of bubbles from the earlier rainfall that decreased the sound levels measured at the bottom hydrophone in the latter measurement. The temperature study provides a third possibility: This hysteresis could have been caused by the surface water reaching raindrop temperatures from the accumulated deposit from the earlier rainfall. With less temperature *difference* during the later rainfall, there would have been lower sound levels, as observed.

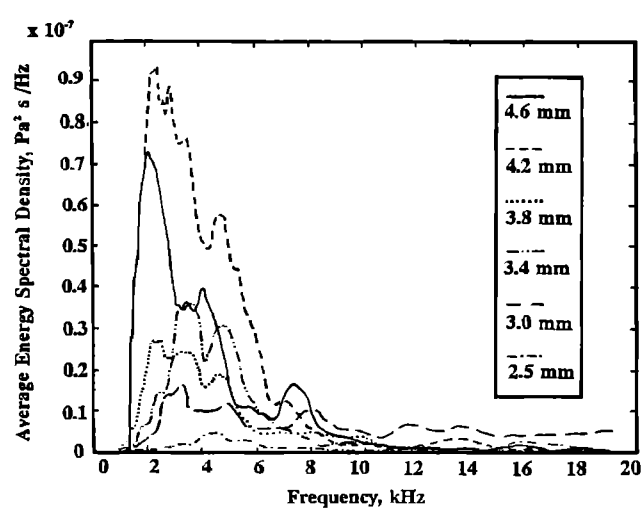

FIG. 11. Average energy spectral densities per drop for large, terminal-speed, drops in 35 ppt salt water (over 500 drops used).

E. Effect of salinity

We have made measurements of water drops falling on both fresh and saline water. In the experiment, the tank water was brought to 35 ppt salinity by the addition of synthetic

sea salt. Then about 30 drops were used for each of four different drop diameters.

The result was that (for water drops of the same temperatures as the tank water) there was a linear decrease of sound energy with increasing salinity. The percentage of bubbles created by drops was the same as for fresh water. However, the *energy* radiated per bubble-producing drop for fresh water was reduced by 40% to 48% for the four different large drop diameters (3.6, 4.0, 4.2, 4.6 mm) in 35 ppt salt water. Otherwise stated, average energy spectral densities for large drops are 3 to 4 dB less in salt water than in fresh water. Scofield (1992) finds that this is due to a lower initial acoustic pressure of the bubble formed in salt water. The probability of type II bubble formation appears to be independent of the salt content of the water (Jacobus, 1991).

VI. PREDICTIONS OF UNDERWATER SOUND SPECTRA, AND INVERSION TO DETERMINE RAINFALL RATES

The previous three sections begin to provide the elements needed to predict underwater sound from a knowledge of the drop size distribution. The average *energy spectral densities* at 1 m from the surface are curves such as in Fig. 11. When the drop size distribution is known for a given rainfall we can calculate the *intensity spectral density* at 1 m from the surface.

A comparison of our drop-acoustic model and measurements at sea is shown in Fig. 13 (Ostwald, 1992). For the model, only the total rainfall rate was known, and it was necessary to assume a Marshall–Palmer drop size distribution. The raindrop temperature was unknown. Nor was the spatial patchiness of the rainfall known. A scattering correction was made for the fact that the hydrophone was mounted in a concrete pad on the seafloor but the hydrophone calibration was not reliable for frequencies less than 5 kHz. Only mid-size and large raindrops were assumed.

Furthermore, the model prediction may be affected by our lack of knowledge of the dependence of type II phenomena on ocean surface roughness during rainfall. For example,

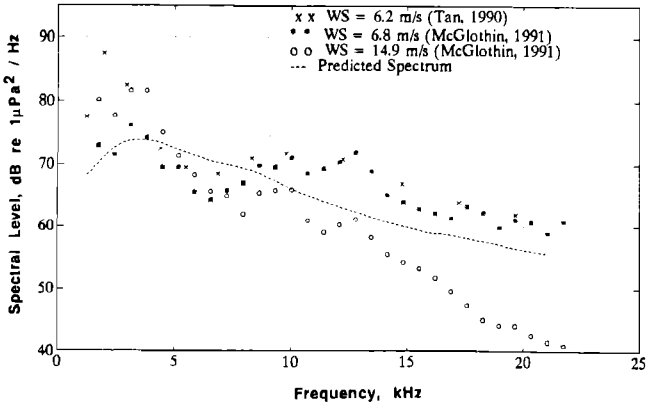

FIG. 13. Predicted intensity spectral density levels at sea, using mid-size and large drops, during 100-mm/h heavy rainfall (dashed line). The ocean spectra were measured by a bottomed hydrophone for three different wind conditions during the same rainfall rate.

it is well known that a surface is "knocked down," i.e., flattened, during rainfall (see Tsimplis and Thorpe, 1989; and Nystuen, 1990) but there is not enough understanding of the water surface during heavy rainfall and we do not know how bubble production from large drops is influenced by the slope and character of the surface in the presence of splash effects from nearby drops.

Nevertheless, the agreement between our model and ocean measurements is quite good, particularly between 3 and 12 kHz, the realm of type II microbubbles. The only serious divergence between the two is in the frequency range from 10 to 22 kHz, during wind speed 14.9 m/s. Such a wind is known to produce whitecaps with large bubble production. There will be dense convective cells of microbubbles under the surface, which will result in significant attenuation of sound propagating to a bottomed hydrophone. The attenuation would be expected to increase with increasing frequency. This could explain the observed divergence for the high wind speed case.

It will be a simple task to invert this sound density spectrum at the surface and thereby to determine the rainfall distribution and total rainfall rate. Jacobus (1991) has performed a trial inversion and Ostwald (1992) has studied the effect of noise on the inversion mathematics.

VII. AIR–SEA GAS TRANSFER BY RAINFALL

The knowledge of percentage production of bubbles of various sizes for a given rainfall rate allows us to calculate the air volume transferred into the water by the bubbles created by the rain. We do not address the subsequent diffusion of air through the bubble walls or the loss of air volume by buoyant return of the bubbles to the air–water interface.

We assume that the spectral peak for each drop diameter occurs because of resonant bubbles, and we obtain their radii from Eq. (12), see Clay and Medwin (1977), Chap. 6,

$$f_0 = \frac{1}{2\pi a_0}\sqrt{\frac{3\gamma P}{\rho_0}}, \tag{12}$$

where f_0 is the resonance frequency, a_0 is the bubble radius at resonance, γ is the ratio of specific heats of the bubble gas, P is the ambient pressure, and ρ_0 is the density of the water.

Consider the case of 92 mm/h. One first obtains the number of drops per square meter of surface per second (DRD) within bands of diameter by multiplying the drop size distribution DSD from Fig. 1 by the appropriate terminal speeds. The fraction of drops creating bubbles is in Fig. 9 for large drops and in Medwin *et al.* (1990) for small drops. The volume per bubble comes from Eq. (12) for the peak frequency. The results shown in Table II make it clear that the major air injection occurs for large drops. For this case the maximum gas transfer occurs for drop diameter 4.2 mm.

It is of interest to compare the air injection by bubbles created by rainfall with that due to breaking waves. The bubble air injection during the very heavy rainfall TRR = 92 mm/h has been calculated as 1.1 $cm^3\ m^{-2}\ s^{-1}$ (Table II). This is much less than the bubble air injection that we have calculated by adding the contributions from Fig. 12 of Toba (1961) for breaking waves in a flume where wind speeds of

TABLE II. Gas injection during heavy rain (92 mm/h). Type I bubbles are assumed to be created by 10% of small drops. Type II bubbles (large drops) are assumed to be produced at the same percentage as for normal incidence onto smooth water.

Drop diameter (mm)	DRD(D) drops $m^{-2} s^{-1}$	Bubble radius (mm)	Percent bubble production	Volume contribution $cm^3 m^{-2} s^{-1}$
0.8	341	0.217	10%	0.0015
0.9	310	0.217	10%	0.0013
1.0	312	0.217	10%	0.0013
1.1	315	0.217	10%	0.0013
2.3	160	0.215	9%	0.0006
2.4	128	0.243	10%	0.0008
2.5	116	0.272	15%	0.0015
2.6	104	0.304	18%	0.0022
2.7	293	0.361	24%	0.0139
3.1	193	0.500	40%	0.0404
3.4	152	0.650	55%	0.0962
3.6	79	0.774	60%	0.0919
4.0	41	1.354	61%	0.2614
4.2	28	1.711	55%	0.3276
4.6	21	1.806	49%	0.2495
	Small drops:	0.005		
	Large drops:	1.086		
	Total:	1.091	$cm^3 m^{-2} s^{-1}$	

8.7 and 12.1 m/s give 8 and 170 $cm^3 m^{-2} s^{-1}$, respectively.

A similar conclusion can be based on ocean observations (Updegraff and Anderson, 1991) of 40 "spillers" during 30 min (i.e., 0.022 wavelets/s) during wind speeds of 1.5 to 2.1 m/s measured 1.5 m over the ocean surface. The ocean microbubble production was virtually the same as during the laboratory experiment of Medwin and Daniel (1990) in which bubble gas injection of 23 cm^3/m^2 was measured for each spiller. Combining the two pieces of data, the ocean spillers at low wind speeds 1.5 to 2.1 m/s caused bubble air injection $(23)(0.022) = 0.5\ cm^3 m^{-2} s^{-1}$. This is comparable to the very heavy rainfall value 1.1 $cm^3 m^{-2} s^{-1}$.

One notes that there are much larger bubbles created in breaking waves than in rainfall, i.e., bubbles up to radii 6 mm in Toba (1961) and 7.4 mm in Medwin and Daniels (1990) compared to 1.8 mm created by large drops in rainfall. It is the volume of the largest bubbles that determines the total bubble gas injection. However, large bubbles would not be entrained to depth as effectively as small bubbles near the turbulent water surface.

VIII. CONCLUSIONS

Underwater sound due to rainfall can be ascribed to three acoustically distinctive ranges of drop diameters, defined as "small" (0.8–1.1 mm), "mid-size" (1.1–2.2 mm), and "large" drops (diameter > 2.2 mm).

Small drops radiate primarily from damped oscillations of microbubbles at frequencies of 13 to 21 kHz with a mean frequency of 15 kHz, but percentage bubble production depends on local angle of incidence.

Mid-size drops radiate only broad band impact sound.

Large drops radiate both impact and bubble sounds. The frequency of the peak energy spectral density of large drops ranges from 1.8 to 8.5 kHz for drop diameters of 4.8 to 2.2 mm, respectively. The percentage of primary (dominant) bubbles created by large drops entering water at normal incidence is a slowly changing function of drop diameter ranging from 0% to 62%. The impact and bubble acoustic energies per unit volume of large drops are functions of drop diameter. Additional acoustic energy of large drops is directly proportional to the absolute difference between surface temperature and drop temperature. The acoustic energy radiated in saline water is 3 to 4 dB less than in fresh water.

There is acceptable agreement between predictions of the raindrop model and ocean measurements during heavy rainfall.

Inversion of underwater sound spectra to obtain rainfall drop distributions appears to be feasible.

The air–sea gas transfer by bubbles created by rainfall is readily obtainable from a knowledge of drop size distribution.

ACKNOWLEDGMENTS

Lt. Chris Scofield assisted with some of the measurements. High-speed photography was provided by Mark Mattivi and Dominic Hart of the Brooks Institute of Photography. Duncan Blanchard guided us to the literature of rainfall measurements at sea. Valuable discussions were held with Ray Kamada concerning the meteorological implications of the dependence of sound intensity on raindrop-surface temperature. Filtered sea water was generously provided by the Monterey Bay Aquarium. The financial assistance of the Office of Naval Research (for H.M.), and the Naval Research Laboratory Detachment at Stennis Space Center and the Naval Postgraduate School Research Office (for J.A.N.) have made this work possible.

Beard, K. V., Johnson, D. B., and Baumgardner, D. (1986). "Aircraft observations of large raindrops in warm, shallow convective clouds," Geophys. Res. Lett. 13, 991–994.

Bom, B. (1969). "The effect of rain on underwater noise levels," J. Acoust. Soc. Am. 45, 150–156.

Clay, C. S., and Medwin, H. (1977). *Acoustical Oceanography* (Wiley, New York).

Franz, G. (1959). "Splashes as sources of sounds in liquids," J. Acoust. Soc. Am. 31, 1080–1096.

Guo, Y. P., and Ffowcs-Williams, J. E. (1991). "A theoretical study on drop impact sound and rain noise," submitted to J. Fluid Mech.

Heindsman, T. E., Smith, R. H., and Arneson, A. D. (1955). "Effect of rain upon underwater noise levels," J. Acoust. Soc. Am. 27, 378–279.

Huske, R. E. (Ed.) (1959). *Glossary of Meteorology* (American Meteorology Society, Boston, MA), 638 pp.

Jacobus, P. W. (1991). "Underwater sound radiation from large raindrops," M. S. thesis, Naval Postgraduate School, Monterey, CA 93943.

Kamada, R. (1992). Personal Communication.

Kurgan, A. (1989). "Underwater sound radiated by impacts and bubbles created by raindrops," M. S. thesis, Naval Postgraduate School, Monterey, CA 93943.

Laville, F., Abbott, G. D., and Miller, M. J. (1991). "Underwater sound generation by rainfall," J. Acoust. Soc. Am. 89, 715–721.

Lemon, D. D., Farmer, D. M., and Watts, D. R. (1984). "Acoustic measurements of wind speed and precipitation over a continental shelf," J. Geophys. Res. 89, 3462–3472.

Longuet-Higgins, M. S. (1990). "An analytical model of sound production by raindrops," J. Fluid Mech. 214, 395–410.

Marshall, J. S., and Palmer, W. (1948). "The distribution of raindrops with size," J. Meteorol. 5, 165–166.
McGlothin, C. C., Jr. (1991). "Ambient sound in the ocean induced by heavy precipitation and the subsequent predictability of rainfall rate," M. S. thesis, Naval Postgraduate School, Monterey, CA 93943.
Medwin, H. (1990). "The oceanic world of infant and adult microbubbles," J. Acoust. Soc. Am. Suppl. 1 88, S1.
Medwin, H., and Beaky, M. M. (1989). "Bubble sources of the Knudsen sea noise spectrum," J. Acoust. Soc. Am. 83, 1124–1130.
Medwin, H., and Daniel, A. C., Jr. (1990). "Acoustical measurements of bubble production by spilling breakers," J. Acoust Soc. Am. 88, 408–412.
Medwin, H., Kurgan, A., and Nystuen, J. A. (1990). "Impact and bubble sound from raindrops at normal and oblique incidences," J. Acoust. Soc. Am. 88, 413–418.
Nystuen, J. A. (1986). "Rainfall measurements using ambient noise," J. Acoust. Soc. Am. 79, 972–982.
Nystuen, J. A., and Farmer, D. M. (1987). "The influence of wind on the underwater sound generated by light rain," J. Acoust. Soc. Am. 82, 270–274.
Nystuen, J. A., and Farmer, D. M. (1989). "Precipitation in the Canadian Atlantic storms program: Measurements of the acoustic signatures," Atmosphere-Ocean 27, 237–257.
Nystuen, J. A. (1990). "A note on the attenuation of surface gravity waves by rainfall," J. Geophys. Res. 95, No. C10, 18 353–18 355.
Nystuen, J. A. (1992). "An explanation of the sound generated by light rain in the presence of wind," to appear in *Natural Physical Sources of Underwater Sound*, edited by B. R. Kerman (Kluwer Academic, Dordrecht, Holland).
Nystuen, J. A., Ostwald, L. H., and Medwin, H. (1992). "The hydroacoustics of a drop impact," J. Acoust. Soc. Am. 92, 1017–1021.
Oguz, H. N., and Prosperetti, A. (1990). "Bubble entrainment by the impact of drops on liquid surfaces," J. Fluid Mech. 218, 143–162.
Ostwald, L. H. (1992). "Predicting the underwater sound of moderate and heavy rainfall from laboratory measurements of radiation from single large water drops," M. S. thesis, Naval Postgraduate School, Monterey, CA 93943.
Pruppacher, H. R., and Klett, J. D. (1978). *Microphysics of Clouds and Precipitation* (Reidel, Dordrecht, Holland).
Pruppacher, H. R., and Pitter, R. L. (1971). "A semi-empirical determination of the shape of cloud and rain drops," J. Atmos. Sci. 28, 86–94.
Pumphrey, H. C., Crum, L. A., and Bjorno, L. (1989). "Underwater sound produced by individual drop impacts and rainfall," J. Acoust. Soc. Am. 85, 1518–1526.
Pumphrey, H. C., and Crum, L. A. (1990). "Free oscillations of near-surface bubbles as a source of the underwater noise of rain," J. Acoust. Soc. Am. 87, 142–148.
Pumphrey, H. C., and Elmore, P. A. (1990). "The entrainment of bubbles by drop impacts," J. Fluid Mech. 220, 539–567.
Schlichting, H. (1960). *Boundary Layer Theory* (McGraw-Hill, New York), p. 168.
Scofield, C. (1992). "Oscillating microbubbles created by water drops falling on fresh and salt water: Amplitude, damping and the effects of temperature and salinity," M. S. thesis, Naval Postgraduate School, Monterey, CA 93943.
Scott, J. C. (1975). "The role of salt in whitecap persistence," Deep-Sea Res. 22, 653–657.
Scrimger, J. A., Evans, D. J., McBean, G. A., Farmer, D. M., and Kerman, B. R. (1987). "Underwater noise due to rain, hail and snow," J. Acoust. Soc. Am. 81, 79–86.
Scrimger, J. A., Evans, D. J., and Yee, W. (1989). "Underwater noise due to rain - open ocean measurements," J. Acoust. Soc. Am. 85, 726–731.
Snyder, D. E. (1990). "Characteristics of sound radiation from large raindrops," M. S. thesis, Naval Postgraduate School, Monterey, CA 93943.
Tan, C. (1990). "A characterization of underwater sound produced by heavy precipitation," M. S. thesis, Naval Postgraduate School, Monterey, CA 93943.
Toba, Y. (1961). Mem. College Sci., Univ. Kyoto, Ser. A XXIX (3), 313–344.
Tsimplis, M., and Thorpe, S. A. (1989). "Wave damping by rain," Nature 342, 893–895.
Updegraff, G. E., and Anderson, V. C. (1991). "Bubble noise and wavelet spills recorded 1 m below the ocean surface," J. Acoust. Soc. Am. 89, 2264–2279.
Worthington, A. M. (1908). *A Study of Splashes* (Longmans, Green, London).